

Supporting Information

Supported Pyridylimine-Cobalt Catalyst for *N*-Formylation of Amines Utilizing CO₂

Naved Akhtar, Manav Chauhan, Poorvi Gupta, Neha Antil, Kuntal Manna*

Department of Chemistry, Indian Institute of Technology Delhi, Hauz Khas, New Delhi 110016, India

*Email: kmanna@chemistry.iitd.ac.in

Table of contents

1. General experiment	S2
2. Synthesis and characterization of pyrim-UiO-68 MOF	S3
3. Post synthetic metalation of pyrim-UiO-68 MOF	S5
4. Pyrim-MOF-Co(THF) catalysed <i>N</i>-formylation of amines	S7
5. Kinetics study for <i>N</i>-formylation of amines	S13
6. GC-MS analysis of the products	S13
7. X-ray absorption spectroscopic analysis	S16
8. DFT calculations	S22
9. XPS analysis	S27
10. References	S30

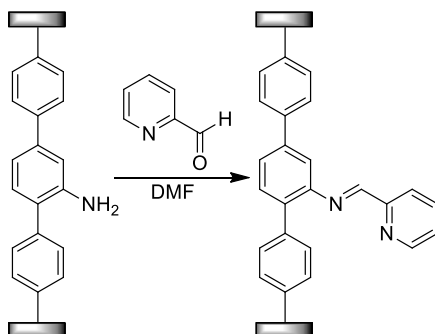
1. General experiment. All the experiments were performed under inert conditions inside the glovebox, except if any case was demonstrated. All the solvents were purchased from Finar and used without further purification. Tetrahydrofuran was dried with calcium hydride followed by distillation over Na/benzophenone. All the reagents are commercially available and used directly as received. 2,5-dibromoaniline was purchased from Alfa Aesar, and $ZrCl_4$ was purchased from Sigma Aldrich. 1H NMR spectra were recorded on a Bruker NMR 500 DRX spectrometer at 500 MHz and referenced to the proton resonance resulting from $DMSO-d_6$ (δ 2.5). Thermogravimetric analysis (TGA) was performed on a PerkinElmer TGA7 system on well-ground samples in a flowing nitrogen atmosphere with a heating rate of 10 °C/min with a range of 40-800 °C. Room temperature powder X-ray diffraction data were collected on a Bruker Advance diffractometer using Ni-filtered $Cu\ K\alpha$ radiation ($\lambda = 1.5406\ \text{\AA}$). Data were collected with a step size of 0.05° and at count time of 1s per step over the range $4^\circ < 2\theta < 70^\circ$. The experimental and simulated PXRD patterns are in good agreement indicating the monophasic nature of the bulk samples. For powder X-ray diffraction measurement of MOFs, moist sample was mounted on a PXRD groove. After catalysis, pyrim-UiO-Co was recovered after centrifugation and stored in THF. Just before the PXRD measurement, the THF was removed, and the moist sample was mounted on a PXRD groove. The catalysis was carried out without any mechanical stirring, and the recovered MOF was not dried before the measurement of PXRD to prevent any mechanical degradation and pore collapse of the MOF. In the case of product analysis of the liquid phase using GC-MS, the following chromatographic conditions were employed; carrier gas: He, flow rate: 1 mL min⁻¹, injection volume: 5.0 μ L, column oven temperature was initially 80.0 °C and then increased up to 230 °C with the rate of 5 °C per minute, and detector temperature was 250 °C. The hydrogen gas evolution was analyzed by a Centurion GC (CS5800) equipped with Porapak Q column in sequence with molecular sieves column and a Thermal conductivity detector (TCD). The chromatographic conditions are as follows; Carrier gas: Argon, Column: 80 °C, TCD: 200 °C, and Injection temperature: 100 °C. ICP-OES data were obtained with an Agilent 5110 ICP-OES and analyzed using Dichroic Spectral Combiner (DSC). Samples were diluted in a 5% HNO_3 matrix and analyzed with a six-point standard curve over the range from 0.1 ppm to 20 ppm. The correlation coefficient was >0.9990 for all analytes of interest. All the reduction reactions were performed using 100 mL Parr pressure vessels (4793 (VGR)-T-SS-3000-DVD). The vessel was pressurized directly from a CO_2 gas tank using a gauge (0-3000 psi displayed, 0-200 bar). To analyse the chemical state of transition elements XPS were recorded on an X-ray photoelectron spectrometer, PHI 5000 VersaProbe III using $Al-K\alpha$ ($h\nu = 1486.6\ eV$) X-ray source. MOF samples were vacuum

dried at room temperature, and then powder samples were measured ultra-high vacuum environment. The morphology and chemical compositions were analysed with a Zeiss Fe-SEM ultra plus55 operating at 20 KV. After vacuum drying, a very small amount of the powder samples of MOF (1-2 mg) were dispersed on the carbon tape for FE-SEM imaging.

2. Synthesis and characterization of pyridylimine-functionalized UiO-68 MOFs.

2.1. Synthesis of UiO-68-NH₂ MOF.¹ First, H₂TPDC-NH₂ (2'-amino-[1,1':4',1''-terphenyl]-4,4''-dicarboxylic acid) was synthesized following a modified procedure.^{2, 3} H₂TPDC-NH₂ (0.010 g, 0.03 mmol) and benzoic acid (0.073 g, 0.6 mmol) were dissolved in a DMF solution (1.22 ml) followed by the addition of ZrCl₄ (0.007 g, 0.03 mmol). The resulting mixture was sonicated for a few minutes and then kept it in a preheated oven at 70 °C for 3 d. After cooling to room temperature, the crystalline solid was isolated by centrifugation and washed it with DMF several times to afford UiO-68-NH₂ MOFs in 41% yield.

2.2. Post synthetic modification of synthesized UiO-68-NH₂ MOF.⁴



In a 1.5 ml centrifuge tube inside the glovebox, synthesized UiO-68-NH₂ MOF was taken in 1ml of deoxygenate DMF followed by the addition of 2-pyridinecarboxaldehyde (20 μ l, 0.210 mmol). The resulting mixture was left overnight with periodic shaking followed by multiple washing of MOF with DMF resulted in pyrim-UiO MOF as light brown solid.

2.3. Analysis of digested pyrim-UiO MOF by ^1H NMR. Digestion of pyrim-UiO MOF was carried out by charging the synthesized UiO MOF into vial containing 0.5 mL of $\text{DMSO-}d_6$, followed by the addition of saturated solution of K_3PO_4 in D_2O with periodic shaking of the resulting mixture. The top organic layer of $\text{DMSO-}d_6$ was then separated out and analysed by ^1H NMR. The ^1H NMR spectrum of digested pyrim-UiO MOF in Figure S1 showed the presence of about 95% pyridylimine moiety along with and 5% TPDC- NH_2^{2-} and 2-pyridinecarboxaldehyde. We thus conclude that the condensation reaction between amine-tagged UiO-68 MOF (UiO-68-NH_2) with 2-pyridinecarboxaldehyde in DMF at room temperature gave the corresponding pyridylimine-functionalized UiO-68 MOF (pyrim-UiO) in 100% conversion, in which all the amino groups were converted to the corresponding pyridylimine. 5% Pyridylimine were hydrolyzed during the digestion process in D_2O as revealed by the presence of TPDC- NH_2^{2-} and 2-pyridinecarboxaldehyde in 1:1 ratio in the ^1H NMR spectrum.

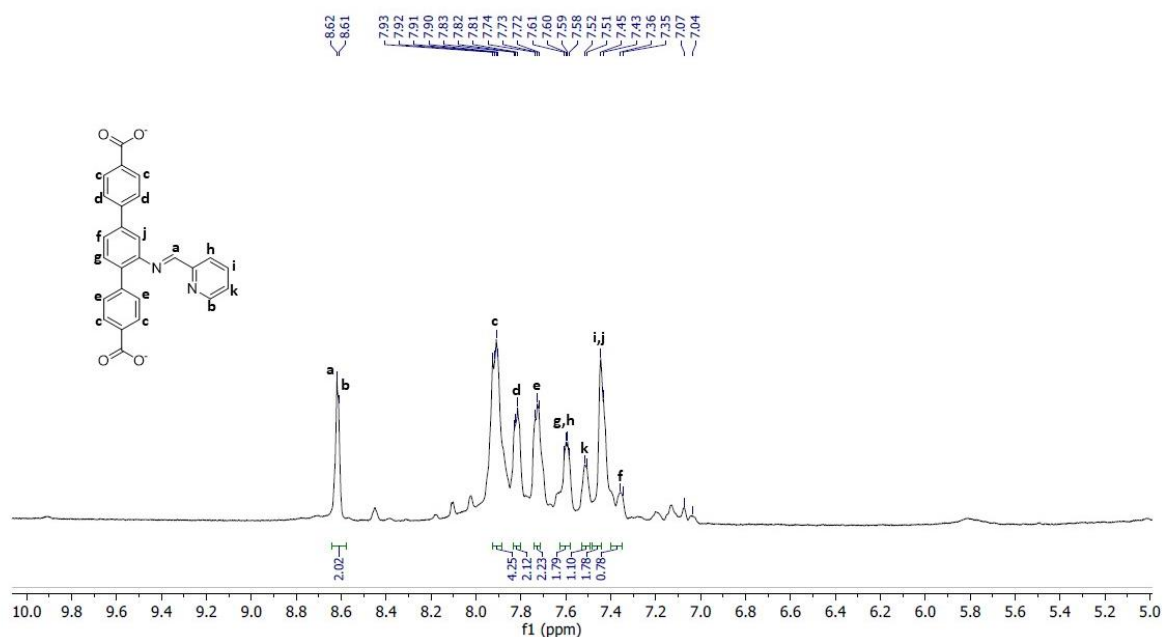
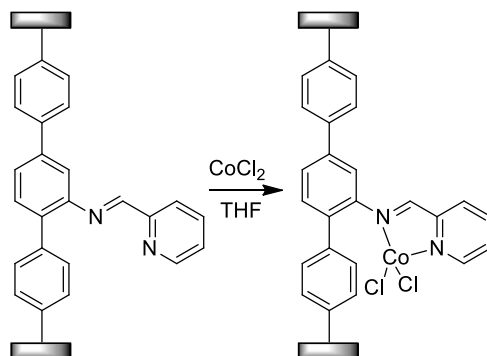


Figure S1. ^1H NMR spectrum (500 MHz, $\text{DMSO-}d_6$) of pyrim-UiO MOF digested in $\text{K}_3\text{PO}_4/\text{D}_2\text{O}/\text{DMSO-}d_6$.

3. Post synthetic metalation of pyrim-MOFs.⁵

3.1. Synthesis of pyrim-UiO-CoCl₂.



Pyrim-UiO MOF (0.030 g, 0.009 mmol) in THF was charged into a vial, and then 1 mL THF solution of CoCl₂ (0.007 g, 0.054 mmol) was added to it. The mixture was stirred slowly overnight at rt. The resultant blue-green solid was centrifuged out of suspension and washed with THF 4-5 times. Pyrim-UiO-Co has 28% solvent weight based on TGA analysis and 38% Co-loading based on ICP-MS analysis.

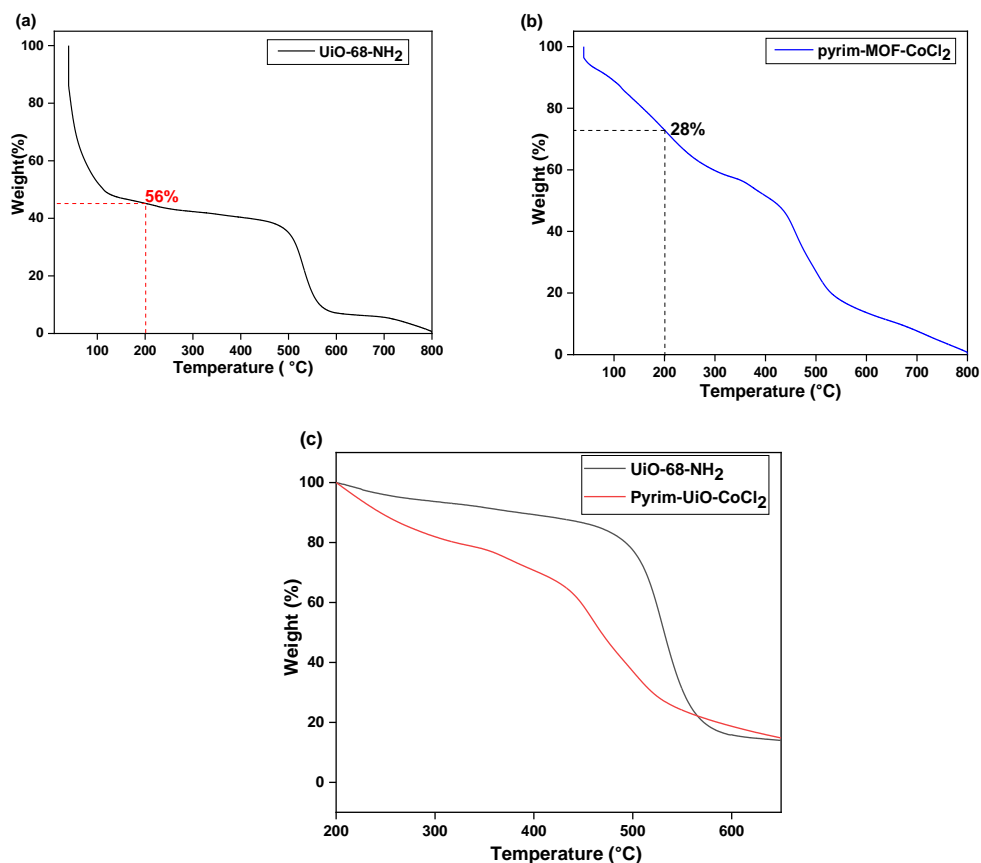


Figure S2. TGA curve of freshly prepared (a) UiO-68-NH₂ and (b) pyrim-UiO-CoCl₂. A solvent weight loss of 56% was observed in (a) and 28% in (b) the room temperature from 40 °C to 200 °C range. (c) TGA curve of freshly prepared UiO-68-NH₂ (black) and pyrim-UiO-CoCl₂ (red) from 200-650 °C. The increased weight of metalated MOF is due to the presence of cobalt within the MOF.

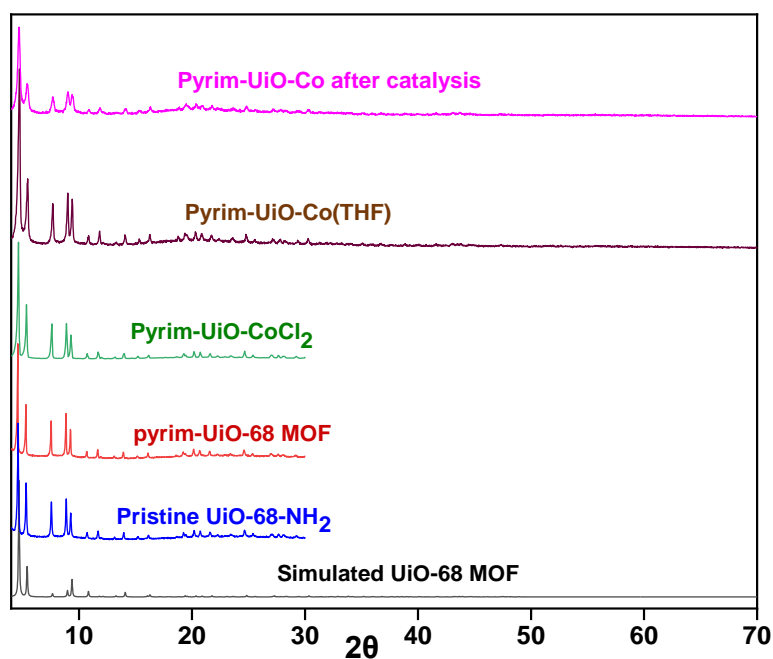
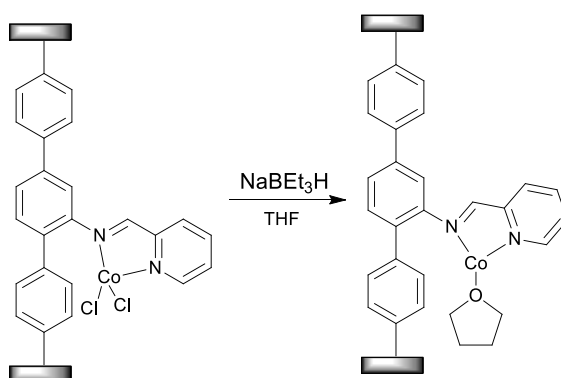


Figure S3. PXRD patterns of simulated UiO-68 MOF (black) and as-synthesized UiO-68-NH₂ MOF (blue), pyrim-UiO-68 MOF (red) and pyrim-UiO-CoCl₂ (green), pyrim-UiO-Co(THF) (brown) and pyrim-UiO-Co after catalysis (magenta).

3.2 Synthesis of pyrim-UiO-Co(THF).⁵

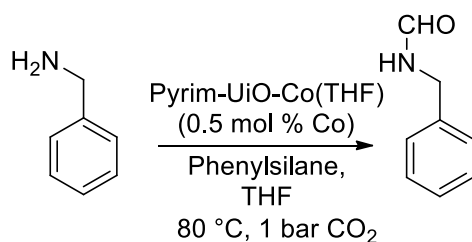


Pyrim-UiO-CoCl₂ (0.015 g, 0.00378 mmol) was charged into a vial containing 3 ml of THF. NaEt₃BH (15 μ L, 1 M in toluene) was added dropwise to the vial, and the mixture was stirred gently for 1 h at room temperature to give pyrim-UiO-Co as black colored solid. The resultant MOF catalyst was separated via centrifugation and then washed with THF several times. Pyrim-MOF-Co(THF) was then used directly for the catalysis.

4. Catalytic reactions with pyrim-UiO-Co(THF).

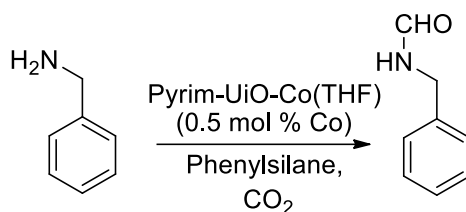
4.1. General procedure for pyrim-UiO-Co(THF) catalysed N-formylation of amines using phenyl silane. In the glovebox, pyrim-UiO-Co(THF) (0.5 mol % of Co) in 3 ml THF was transferred into 50 ml glass liner. Then phenyl silane along with amine containing substrate were added in to the liner. Then, the liner was fitted in a high pressure reactor followed air tight sealed. The sealed Parr reactor was taken out from the glovebox and purged with CO₂ for 2 to 3 times. The Parr reactor was pressurized to 1-20 bar CO₂ and kept on heating at 80 °C for 16 to 36 h. After the reaction was completed the solid MOF was removed with the help of centrifugation from the suspension inside the glovebox followed by several washing with THF and can be reused. The remaining organic extract in the suspension were concentrated in vacuo to yield corresponding N-formylated as the pure product.

4.2. A Typical procedure for pyrim-UiO-Co(THF) catalysed N-formylation of benzylamine.



Pyrim-UiO-Co(THF) (0.5 mol% of Co) in 3 ml of THF was transferred into a 50 mL glass liner in a glovebox. To the mixture, benzylamine (40 μ L, 0.375 mmol) and 80 μ L phenylsilane were added. Then, the liner was fitted in a Parr reactor and sealed. The sealed Parr reactor was taken out from the glovebox and purged it with CO₂ gas two to three times. The Parr reactor was pressurized to 1.0 bar CO₂ and stirred at room temperature for 16 h. After the completion of the reaction, the pressure of the reactor was released. The solid MOF was removed from suspension inside the glove box, washed with THF multiple times, and reused. The combined organic extracts were concentrated in vacuo, followed by column chromatography using hexane and ethyl acetate (50:1, R_f: 0.7) as an eluent to yield N-benzylformamide as the pure product (0.045 g, 0.335 mmol, 89%).

Table S1. Optimization reaction conditions for the *N*-formylation of benzylamine.^a



Entry	Catalyst	Reductant	Temperature (°C)	P _{CO2} (bar)	Time (h)	Solvent	GC-Yield (%)
1	Pyrim-UiO-Co(THF) (0.5 mol%)	Phenylsilane (1.5 eq)	25	20	20 h	THF	58
2	Pyrim-UiO-Co(THF) (0.5 mol%)	Phenylsilane (1.5 eq)	50	20	20 h	THF	73
3	Pyrim-UiO-Co(THF) (0.5 mol%)	Phenylsilane (1.5 eq)	100	20	20 h	THF	78
4	Pyrim-UiO-Co(THF) (0.5 mol%)	Phenylsilane (1.5 eq)	80	20	16 h	THF	85
5	Pyrim-UiO-Co(THF) (0.5 mol%)	Phenylsilane (2 eq)	80	20	16 h	THF	91
6	Pyrim-UiO-Co(THF) (0.5 mol%)	Phenylsilane (2 eq)	80	10	16 h	THF	92
7	Pyrim-UiO-Co(THF) (0.5 mol%)	Phenylsilane (2 eq)	80	5	16 h	THF	92
8	Pyrim-UiO-Co(THF) (0.5 mol%)	Phenylsilane (2 eq)	80	1	16 h	THF	91
9	Pyrim-UiO-Co(THF) (0.5 mol%)	Phenylsilane (2.3 eq)	80	1	16 h	THF	89
10	Pyrim-UiO-Co(THF) (0.5 mol%)	Phenylsilane (2 eq)	80	20	16 h	1,4-Dioxane	86
11	Pyrim-UiO-Co(THF) (0.5 mol%)	Phenylsilane (2 eq)	80	20	16 h	Heptane	62
12	Pyrim-UiO-Co(THF) (0.5 mol%)	Phenylsilane (2 eq)	80	20	16 h	Toluene	69
13	Pyrim-UiO-Co(THF) (0.5 mol%)	(MeO) ₂ MeSiH (2 eq)	80	5	16 h	THF	21
14	No catalyst	Phenylsilane (2 eq)	80	5	16 h	THF	5

4.3. Test for “heterogeneity” of pyrim-UiO-Co(THF) in *N*-formylation of amines.

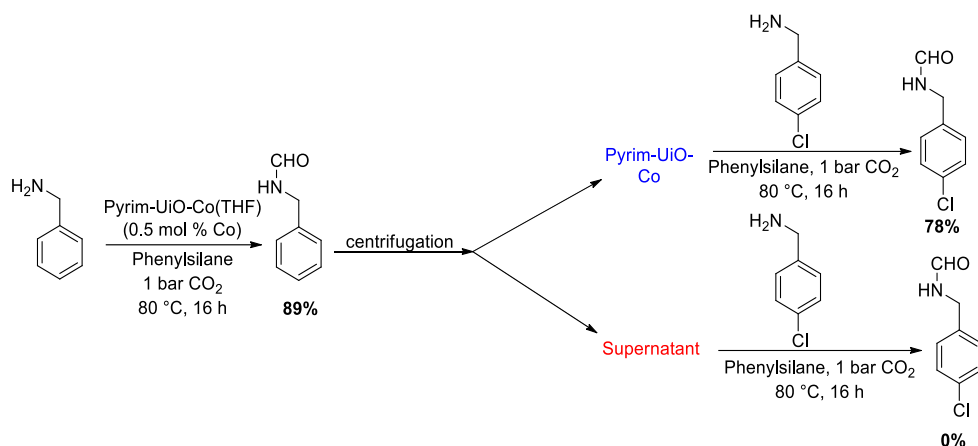


Figure S4. Heterogeneity test of pyrim-UiO-Co(THF) for the *N*-formylation of amines.

Pyrim-UiO-Co(THF) (0.5mol% of Co) in 3 ml of THF was transferred into a 50 mL glass liner in a glovebox. To the mixture, benzylamine (40 μ l, 0.375 mmol) and 80 μ l phenylsilane were added. Then, the liner was fitted in a Parr reactor and sealed. The sealed Parr reactor was taken out from the glovebox and purged it with CO₂ gas two to three times. The Parr reactor was pressurized to 1 bar CO₂ and stirred at 80°C for 16 h. After the completion of the reaction, the pressure of the reactor was released. The solid MOF was removed from suspension to separate the solid and the supernatant, inside the glove box and washed with THF multiple times. The conversion analysed by taking aliquots from the organic extract gave 89% of *N*-benzylformamide.

Two reactions were set up separately in two different Parr reactors, one with the solid and the other one with the supernatant recovered from the previous reaction. The extracted solid and supernatant were added into two separate liners, and *p*-chlorobenzylamine (45 μ l, 0.375 mmol), 90 μ l phenylsilane, and 3 mL of THF were added to each liner. Then both the liners were fitted into two separate Parr reactors and sealed. The sealed Parr reactor was taken out from the glovebox and purged it with CO₂ gas two times. The Parr reactor was pressurized to 1 bar CO₂ and stirred at 80°C for 16 h. After the completion of the reaction, the pressure of the reactors was released. The reactions were analysed with the GC-MS, which showed that the reaction with the solid MOF gave 100% conversion with 78% yield, while the reaction with supernatant gave 0% conversion. This experiment excludes the potential of any leached Co-species responsible for catalysis and confirms that solid pyrim-UiO-Co(THF) was the actual catalyst for the *N*-formylation of amines.

4.4. Hg test. A catalytic *N*-formylation of amine was carried out in the presence of a drop of Hg to investigate the role of any leached Co-nanoparticles in the solution responsible for catalysis. Hg is known to form an amalgam with metallic cobalt, thus removing any in-situ-borne metallic cobalt during catalysis. The details of the experiments are as follows:

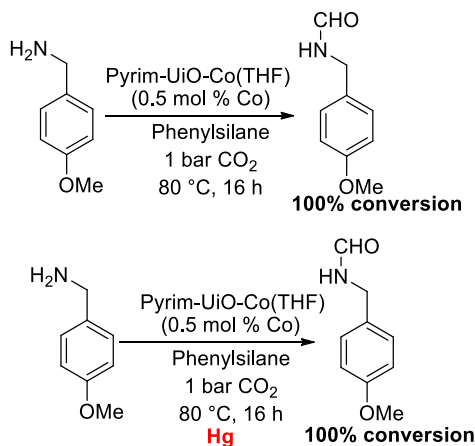


Figure S5. Hg test in the *N*-formylation of *p*-methoxybenzylamine with pyrim-UiO-Co(THF).

Pyrim-UiO-Co(THF) (0.5 mol % of Co) was charged into two separate 3 mL vials and washed with THF multiple times inside the glovebox. The MOF as a slurry in 3 mL THF was transferred to the two separate 50 mL glass liners. *p*-Methoxybenzylamine (51 μ l, 0.375 mmol), 90 μ l phenylsilane and 3 mL of THF was added to both the liners. In one of the reaction mixtures, a drop of mercury was added. Then, the liners were fitted in a Parr reactor and sealed. The sealed Parr reactors were taken out from the glovebox and purged it with CO₂ gas two times, then pressurized with 1 bar CO₂. The reactors were then stirred at 80 °C for 16 h. After the completion of the reaction, the pressure of the reactor was released. The solid MOF was removed from suspension inside the glove box and washed with THF multiple times. The catalytical conversion was 100% for both the reactions analysed by GC-MS. We thus conclude that any leached Co-particles were not responsible for the catalytical activity, and pyrim-UiO-Co(THF) was the actual catalyst.

4.5. Recycling of pyrim-UiO-Co(THF) for the *N*-formylation of benzylamines.

The recycle and reuse experiment was conducted at incomplete conversion (~50-60%) to check the stability of the pyrim-UiO-Co(THF) catalyst at various runs (Table S2). The detailed procedure of recycling experiment is given below.

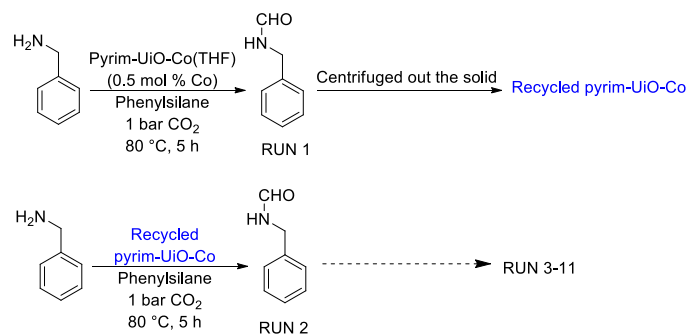


Figure S6. Recycle and reuse of pyrim-UiO-Co(THF) in N-formylation of benzylamine.

Pyrim-UiO-Co(THF) (0.5 mol% of Co) into 3ml vial was taken inside the glovebox and wash it with THF for one to three times. The MOF as a slurry in THF was transferred to the 50 ml glass tube. To the mixture, 3 ml THF and benzylamine (40 μ L, 0.375 mmol) were added, and the glass tube was sealed in a Parr reactor. The Parr reactor was taken out from the glove box and purged two times with the CO₂ gas. The reactor was pressurized with 1 bar CO₂ and heated to 80 °C for 5 h. After cooling the reactor to room temperature, the reactor was taken inside the glove box, and released the pressure. The solid was centrifuged out of the suspension and washed with the THF. The organic extract was concentrated under vacuo to give the pure formylated product. The solid MOF was then recycled.

Inside the glovebox, the recovered MOF-catalyst was again added to the glass tube. 3 ml THF and benzylamine (40 μ L, 0.375 mmol) were added to the glass tube and sealed it in a Parr reactor. The Parr reactor was taken out from the glove box and was purged with the CO₂ gas and then pressurized it to 1 bar of CO₂. The solution was heated at 80 °C for 5 h. After the reaction, the solution was analyzed in the same way as mentioned previously in run 1. The recycling and reuse experiments were performed up to 11 times in total.

Table S2. % GC-Yield of N-benzylformamide, the leaching of Co at various runs of the recycling of pyrim-UiO-Co(THF) in the N-formylation of benzylamine.

No. of Run	Time	%GC-Yield	%Leaching (Co, Zr)
Run-1	5 h	54	0.07, 1.34
Run-2	5 h	56	
Run-3	5 h	59	
Run-4	5 h	51	
Run-5	5 h	52	0.13, 2.11
Run-6	5 h	58	
Run-7	5 h	52	
Run-8	5 h	51	
Run-9	5 h	53	0.14, 2.89
Run-10	5 h	57	
Run-11	5 h	55	

4.6. Investigation of the effect of pore sizes on the rate of catalysis. The effect of pore sizes on the rate of formylation of amine was investigated by comparing the rate of *N*-formylation reactions of amines catalyzed by pyrim-UiO-Co(THF) with that of pyrim-UiO-66-Co under identical reaction conditions. Pyrim-UiO-66-Co has the same topology but smaller pore sizes compared to pyrim-UiO-Co(THF).

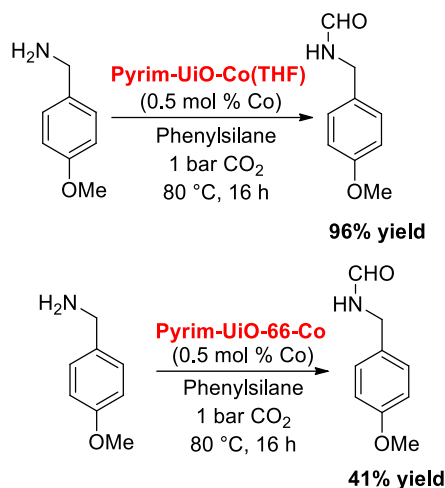


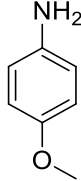
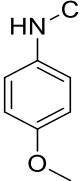
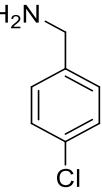
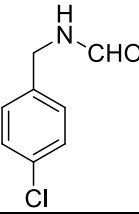
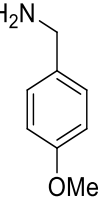
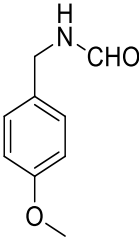
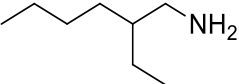
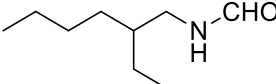
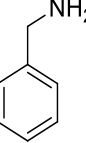
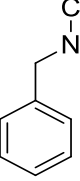
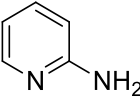
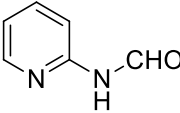
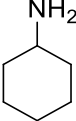
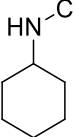
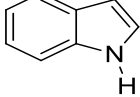
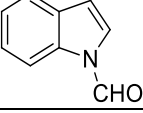
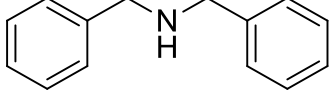
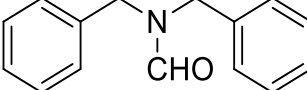
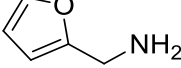
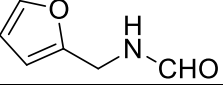
Figure S7. The *N*-formylation of 4-methoxybenzylamine catalyzed by pyrim-UiO-Co(THF) with that of pyrim-UiO-66-Co under identical reaction conditions.

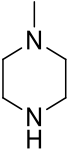
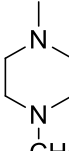
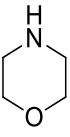
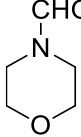
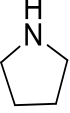
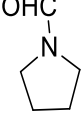
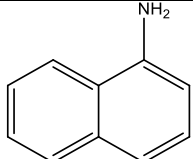
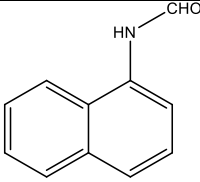
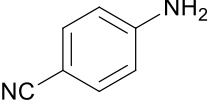
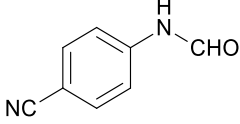
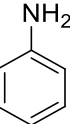
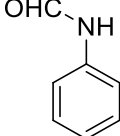
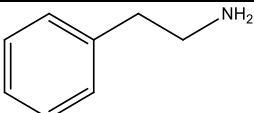
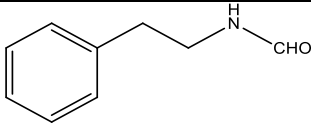
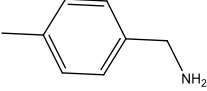
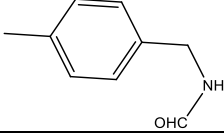
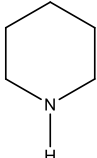
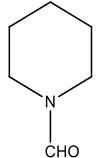
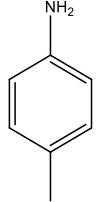
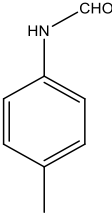
pyrim-UiO-66-Co was synthesized according to the reported procedure.⁵ Two separate 5 ml vials were charged with pre-activated pyrim-UiO-Co(THF) (0.5 mol% of Co) and pyrim-UiO-66-Co (0.5 mol% of Co) each and washed with THF multiple times. Each MOF slurry in 3 ml THF were transferred to two different 50 ml glass liners containing 4-methoxybenzylamine (51 μ l, 0.375 mmol) and 90 μ l of phenylsilane. The liners were fitted into the Parr reactors and sealed properly. The sealed Parr reactors were taken out from the glove box. The reactors were purged twice with the CO₂, then charged with 1 bar CO₂ each and stirred at 80 °C for 16 h. After the completion of the reaction, the pressure from the reactors was released. The solid MOF was then removed from suspension inside the glove box and the combined organic extracts were evaporated and analysed by GC-MS. The catalytical conversions for both the reactions were 100% while, the selectivity to get *N*-(4-methoxyphenyl)formamide were 96% and 41% with pyrim-UiO-Co(THF) and pyrim-UiO-66-Co respectively. This experiment indicates that the larger pore size MOF, pyrim-UiO-Co(THF), was about three times more active than pyrim-UiO-66-Co in formylation of benzyl amine presumably due to the facile diffusion of reactant and product through its larger channels.

5. Determination of the rate law for pyrim-UiO-Co(THF) catalysed *N*-formylation of benzylamine. The rate law for *N*-formylation of benzylamine was determined by the method of initial rates (up to 10% conversion).⁶ The reactions were conducted in THF (total volume of solution was 3.0 mL) in a Parr reactor at 80°C. For each kinetic experiment, a glass liner was charged with MOF-catalyst, benzylamine, phenylsilane and THF under N₂. The liner was fitted in a Parr reactor and sealed properly, pressurized with CO₂ and heated at 80 °C for 30 min. The concentration of the product was analysed by GC-FID using mesitylene as internal standard. The initial rates for the *N*-formylation of benzylamine were measured for several substrate concentrations at constant catalyst concentration. Linear regression fits for [benzylamine] versus time for the first 30 min of the reaction provided the initial rate ($d[\text{benzylamine}]/dt$) for a particular initial substrate concentration. To determine the rate dependence on one reagent, the concentration of that reagent was varied, while the concentration of other reagents, pressure, and the total volume of solution (3.0 mL) were kept constant. The rate dependence on CO₂ pressure was measured, while keeping all the reagents constant and varying CO₂ pressure. The rates refer to the rates of consumption of benzylamine in units of mM·min⁻¹. To determine the rate dependence on the catalyst, the concentration of Co was varied between 6.01×10^{-4} to 2.4×10^{-3} mM, while the initial concentrations of benzylamine were 1.83×10^{-1} mM, concentration of phenylsilane was 1.6×10^{-1} mM and CO₂ pressure was 5 bar. To determine the rate dependence on benzylamine, initial concentration of phenylsilane was 1.6×10^{-1} mM and CO₂ pressure was 5 bar, while the concentration of benzylamine was varied between 9.1×10^{-2} mM to 3.6×10^{-1} mM, while the concentration of Co was 6.01×10^{-4} mM. To determine the rate dependence on pressure of CO₂, the concentrations of benzylamine were 1.83×10^{-1} mM, concentration of phenylsilane was 1.6×10^{-1} mM, and CO₂ pressure was varied from 5-20 bar, while the concentration of Co was 6.01×10^{-4} mM. To determine the rate dependence on phenylsilane, the concentrations of phenylsilane was varied between 2.4×10^{-1} mM to 4.8×10^{-1} mM, while initial concentration of benzylamine were 1.83×10^{-1} mM, concentration of Co was 6.01×10^{-4} mM, and CO₂ pressure was 5 bar.

6. Analysis of products by GC-MS. The conversions and yields of the reactions were determined by Agilent 7890B gas chromatograph equipped with a mass detector (Agilent 5977B GC/MSD) and HP-5MS Ultra Inert 30 m-250 μ m-0.25 μ m column for GC-MS. GC-MS conditions: Inj: 220 °C; Det: 250 °C; Column temp: 80 °C followed by a ramp of 5 °C/min to 220 °C; Column flow: 1.0 mL/min.

Table S3. The GC-MS retention times of the arene substrates and the products.

Entry	Substrate	Retention time	Product	Retention time
1		9.86		18.1
2		9.50		9.92
3		10.95		20.3
4		5.17		13.23
5		5.50		14.3
6		5.23		10.58
7		3.49		11.8
8		11.52		13.6
9		16.30		27.0
10		3.24		9.18

11		3.4		9.42
12		2.98		7.49
13		3.1		6.73
14		17.56		20.05
15		15.55		22.20
16		4.91		12.07
17		7.3		16.07
18		7.37		16.62
19		3.2		7.99
20		6.51		14.90

7.1. X-ray absorption spectroscopic analysis. X-ray Near-Edge Structure (XANES) and Extended X-ray Absorption Fine Structure (EXAFS) measurements have been carried out at the Energy-Scanning EXAFS beamline (BL-9) at the Indus-2 Synchrotron Source at Raja Ramanna Centre for Advanced Technology (RRCAT), Indore, India.⁷ All the measurements were performed at room temperature. This beamline operates in the energy range of 4 keV to 25 keV. The beamline optics consist of a Rh/Pt coated collimating meridional cylindrical mirror and the collimated beam reflected by the mirror is monochromatized by a Si(111) based double crystal monochromator (DCM). The second crystal of the DCM is a sagittal cylindrical crystal which is used for horizontal focusing of the beam while another Rh/Pt coated bendable post mirror facing downward is used for vertical focusing of the beam at the sample position. Two ionization chambers (300 mm length each) have been used for data collection in the transmission mode; one ionization chamber for measuring incident flux, the second one for measuring transmitted flux. For energy calibration, standard metal foils were used. Appropriate gas pressure and gas mixture have been chosen to achieve 10-20% absorption in the first ionization chamber and 70-90% absorption in the second ionization chamber to obtain a better signal-to-noise ratio. Pellets were made from powder samples for recording absorption spectra. Sample powder was mixed homogeneously with cellulose powder in appropriate proportion and pressed (2 Ton) into a 15 mm diameter disc. The amount of the sample was estimated such that to get a reasonable edge jump at a particular absorption edge of the element to be probed. Spectra were collected at the cobalt K-edge in transmission mode and were calibrated against the reference spectrum of metallic cobalt (7709 eV). Data were processed using Demeter software.⁸ A metallic cobalt foil standard was used as a reference for energy calibration and was measured simultaneously with experimental samples.

7.2. XANES analysis. The oxidation state of the Co species within pyrim-UiO-CoCl₂, pyrim-UiO-Co(THF) and pyrim-UiO-Co after catalysis was determined by the comparison of the energies of their pre-edge and K-edge positions to those of CoCl₂. The position of the pre-edge and K-edge of pyrim-UiO-CoCl₂ aligned well with those of CoCl₂. Therefore, we assign the oxidation state of cobalt in pyrim-UiO-CoCl₂ as +2. However, in the case of pyrim-UiO-Co(THF), the pre-edge is at 7706 eV, which is 3 eV lower than that of pyrim-UiO-CoCl₂ and CoCl₂. We thus infer that the oxidation state of cobalt ion in pyrim-UiO-Co(THF) is zero. However, the Co K-edge of pyrim-UiO-Co(THF) is 3 eV higher than that of metallic cobalt(0). The higher Co K-edge energy in XANES of pyrim-UiO-Co(THF) than that of metallic cobalt(0) is attributed to the electron backdonation from $d_{\pi}(\text{Co})$ to $p_{\pi}^*(\text{pyrim})$.

7.3. EXAFS fitting using DFT optimized structures. The spectra were calibrated against the reference spectra and aligned to the first peak in the smoothed first derivative of the absorption spectrum, the background noise was removed, and the spectra were processed to obtain a normalized unit edge step. The fitting parameters of pyrim-UiO-CoCl₂, pyrim-UiO-Co(THF) and pyrim-UiO-Co after catalytic amine formylation are summarized in Table S5, Table S7 and Table S8, respectively.

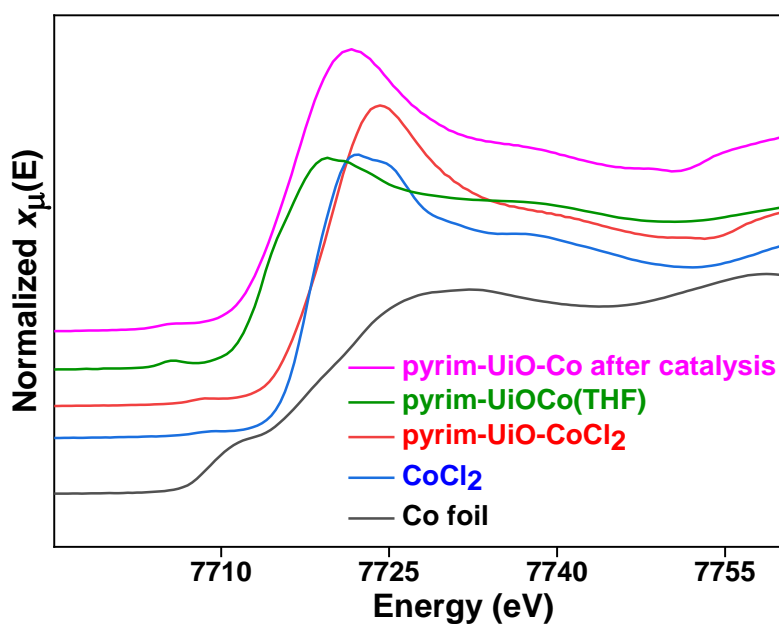


Figure S8. $\mu(E)$ XAS spectra of metallic Co(0) (black), CoCl₂ (blue), pyrim-UiO-CoCl₂ (red), pyrim-UiO-Co(THF) (green), and pyrim-UiO-Co after catalysis (magenta).

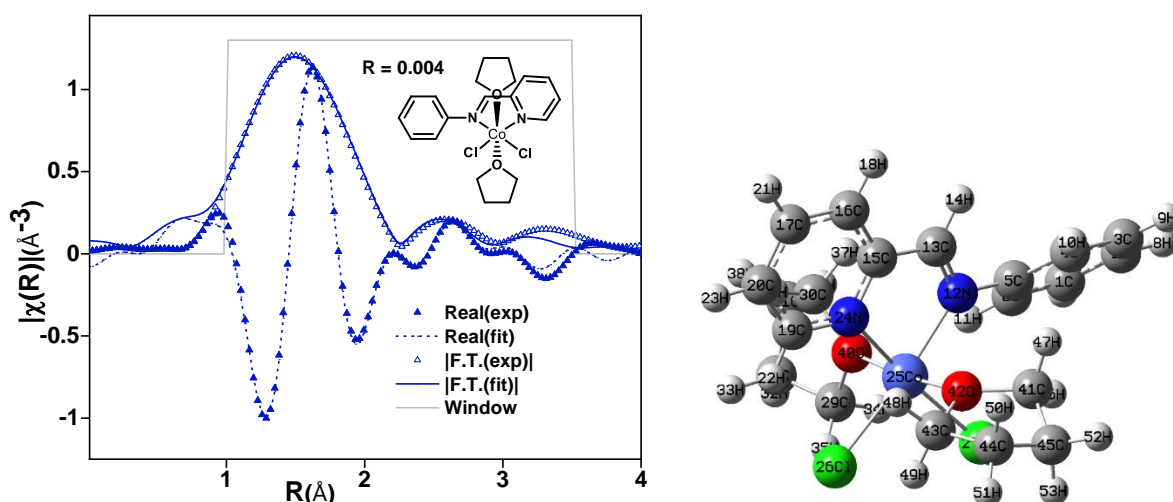


Figure S9. (a) EXAFS spectrum and fit of pyrim-UiO-CoCl₂. (b) DFT-optimized structure of (pyrim)CoCl₂(THF)₂.

Table S4. Atoms coordinates used for EXAFS fitting parameters of pyrim-UiO-CoCl₂(THF)₂

Atom No.	Atomic symbol	Coordinates		
		X	Y	Z
40	O	-4.447735	5.373369	-1.680895
42	O	-4.877530	6.507511	1.762643
24	N	-4.909663	7.654624	-0.641159
12	N	-2.988274	5.804915	0.393602
27	Cl	-4.760357	3.884170	0.741058
26	Cl	-6.839608	5.744080	-0.111420
13	C	-2.415042	7.121739	0.080106
15	C	-3.576187	8.017402	-0.451994
19	C	-5.807343	8.564116	-1.200985
5	C	-1.932672	4.921036	0.908734
29	C	-3.422031	4.424689	-2.284218
30	C	-5.329810	5.888267	-2.809274
43	C	-5.911598	7.471113	1.982044
41	C	-4.268926	6.133321	3.001813

Table S5. Summary of EXAFS fitting parameters of pyrim-UiO-CoCl₂(THF)₂.

Sample	Pyrim-CoCl ₂ (THF) ₂	Fitting range	k 3-13 Å ⁻¹ R 1.0-3.5 Å
Independent points	13	R-factor	0.004
Variables	11	S ₀ ²	0.7
Reduced chi-square	40	ΔE ₀ (eV)	7.8
R(Co-O40)	2.20±0.08	σ ² (Co-O40) (Å ²)	0.003±0.002
R(Co-O42)	2.20±0.08	σ ² (Co-O42) (Å ²)	0.003±0.002
R(Co-N24)	2.05±0.08	σ ² (Co-N24) (Å ²)	0.003±0.002
R(Co-N12)	2.05±0.08	σ ² (Co-N12) (Å ²)	0.003±0.002
R(Co-Cl27)	2.30±0.08	σ ² (Co-Cl27) (Å ²)	0.003±0.002
R(Co-Cl26)	2.30±0.08	σ ² (Co-Cl26) (Å ²)	0.003±0.002
R(Co-C13)	2.80±0.08	σ ² (Co-C13) (Å ²)	0.01±0.001
R(Co-C15)	2.80±0.08	σ ² (Co-C15) (Å ²)	0.01±0.001
R(Co-C19)	3.03±0.02	σ ² (Co-C19) (Å ²)	0.0009±0.0001
R(Co-C5)	3.03±0.02	σ ² (Co-C5) (Å ²)	0.0009±0.0001

R(Co-C29)	3.30±0.09	σ^2 (Co-C29) (\AA^2)	0.006±0.002
R(Co-C30)	3.30±0.09	σ^2 (Co-C30) (\AA^2)	0.006±0.002
R(Co-C43)	3.50±0.1	σ^2 (Co-C43) (\AA^2)	0.0009±0.0001
R(Co-C41)	3.50±0.1	σ^2 (Co-C41) (\AA^2)	0.0009±0.0001

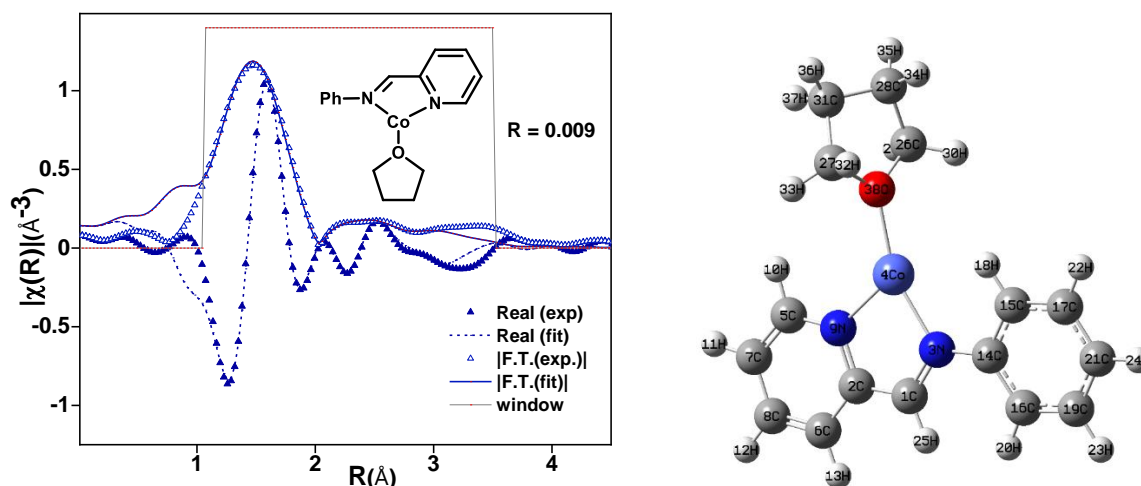


Figure S10. (a) EXAFS spectrum and fit of pyrim-UiO-Co(THF). (b) DFT-optimized structure of pyrim-Co(THF) for EXAFS fitting.

Table S6. Atoms coordinates used for EXAFS fitting parameters of pyrim-UiO-Co(THF).

Atom No.	Atomic symbol	Coordinates		
		X	Y	Z
3	N	-14.374835	-5.415588	-14.024619
9	N	-13.605732	-3.382893	-12.633045
38	O	-14.189606	-1.850014	-15.451178
18	H	-14.963245	-4.928159	-16.493752
1	C	-14.055855	-5.688267	-12.732106
2	C	-13.630021	-4.603214	-11.958672
26	C	-15.317565	-0.924717	-15.486769
27	C	-13.009946	-1.249122	-16.068291
5	C	-13.202945	-2.283393	-11.968703
15	C	-15.101275	-5.974445	-16.235262
33	H	-12.167193	-1.401441	-15.394939
30	H	-16.198516	-1.491432	-15.785424
14	C	-14.813048	-6.382911	-14.910811

Table S7. Summary of EXAFS fitting parameters of pyrim-UiO-Co(THF).

Sample	Pyrim-UiO-Co(THF)	Fitting range	k 3-13 Å ⁻¹ R 1.1-3.5 Å
Independent points	13	R-factor	0.009
Variables	8	S ₀ ²	1.1
Reduced chi-square	140	ΔE ₀ (eV)	2.43
R(Co-N3)	1.92±0.1	σ ² (Co-N3) (Å ²)	0.003±0.002
R(Co-N9)	1.92±0.1	σ ² (Co-N9) (Å ²)	0.003±0.002
R(Co-O38)	1.96±0.09	σ ² (Co-O38) (Å ²)	0.003±0.002
R(Co-H18)	2.57±0.09	σ ² (Co-H18) (Å ²)	0.0004±0.0002
R(Co-C1)	2.76±0.1	σ ² (Co-C1) (Å ²)	0.002±0.001
R(Co-C2)	2.76±0.1	σ ² (Co-C2) (Å ²)	0.002±0.001
R(Co-C26)	2.93±0.1	σ ² (Co-C26) (Å ²)	0.002±0.001
R(Co-C27)	2.93±0.1	σ ² (Co-C27) (Å ²)	0.002±0.001
R(Co-C5)	3.04±0.09	σ ² (Co-C5) (Å ²)	0.0004±0.0002
R(Co-C15)	3.04±0.09	σ ² (Co-C15) (Å ²)	0.0004±0.0002
R(Co-H33)	3.08±0.09	σ ² (Co-H33) (Å ²)	0.003±0.002
R(Co-H30)	3.08±0.09	σ ² (Co-H30) (Å ²)	0.003±0.002
R(Co-C14)	3.13±0.09	σ ² (Co-C14) (Å ²)	0.003±0.002

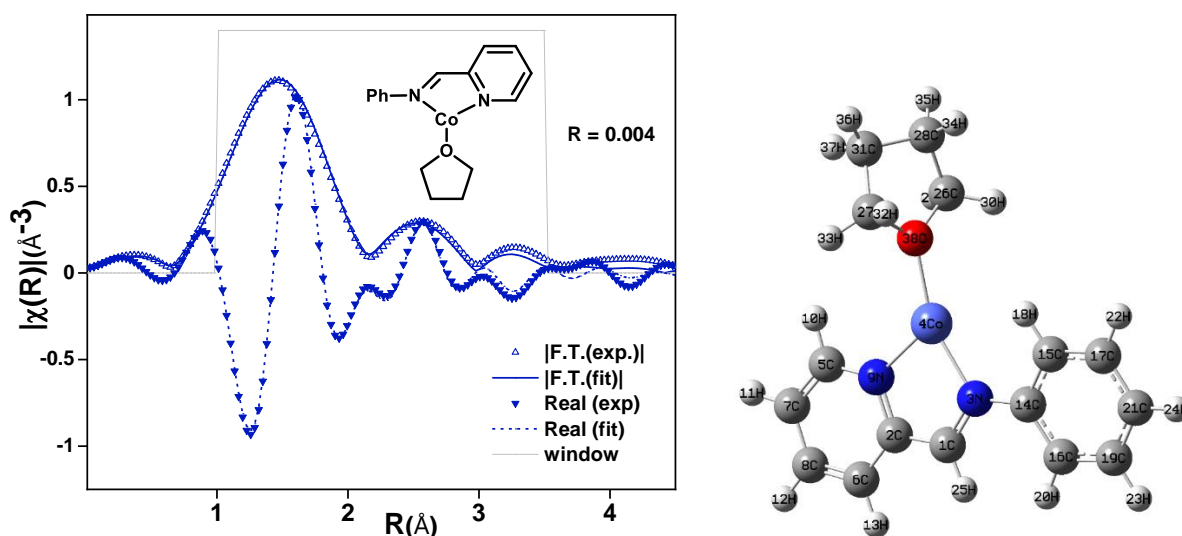


Figure S11. (a) EXAFS spectrum and fit of pyrim-UiO-Co recovered after hydroformylation of benzyl amine with PhSiH₃. (b) DFT-optimized structure of pyrim-Co(THF) for EXAFS fitting.

Table S8. Summary of EXAFS fitting parameters of pyrim-UiO-Co recovered after hydroformylation of benzyl amine with PhSiH₃.

Sample	Pyrim-UiO-Co after catalysis	Fitting range	k 3-13 Å ⁻¹ R 1.1-3.5 Å
Independent points	13	R-factor	0.004
Variables	8	S₀²	1.2
Reduced chi-square	120	ΔE₀(eV)	1.95
R(Co-N3)	1.92±0.1	σ²(Co-N3) (Å²)	0.004±0.003
R(Co-N9)	1.92±0.1	σ² (Co-N9) (Å²)	0.004±0.003
R(Co-O38)	1.96±0.1	σ² (Co-O38) (Å²)	0.004±0.003
R(Co-H18)	2.57±0.1	σ² (Co-H18) (Å²)	0.004±0.003
R(Co-C1)	2.76±0.1	σ² (Co-C1) (Å²)	0.004±0.003
R(Co-C2)	2.76±0.1	σ² (Co-C2) (Å²)	0.004±0.003
R(Co-C26)	2.93±0.1	σ² (Co-C26) (Å²)	0.005±0.003
R(Co-C27)	2.93±0.1	σ² (Co-C27) (Å²)	0.005±0.003
R(Co-C5)	3.04±0.1	σ² (Co-C5) (Å²)	0.004±0.003
R(Co-C15)	3.04±0.1	σ² (Co-C15) (Å²)	0.004±0.003
R(Co-H33)	3.08±0.1	σ² (Co-H33) (Å²)	0.004±0.003
R(Co-H30)	3.08±0.1	σ² (Co-H30) (Å²)	0.004±0.003
R(Co-C14)	3.13±0.1	σ² (Co-C14) (Å²)	0.004±0.003

8. DFT calculations. All quantum chemical calculations were conducted using DFT as implemented in the Gaussian 09 software suite of *ab initio* quantum chemistry programs with B3LYP level of theory. Electronic structure complexes were optimized at the unrestricted level using 6-311G (d,p) basis set.⁹⁻¹³ All energy calculations were performed in solvated state. We used the Polarizable Continuum Model (PCM) using the integral equation formalism variant (IEFPCM) as the default self-consistent reaction field (SCRFF)^{14,15} approach based on accurate numerical solutions of the Poisson-Boltzmann equation by using tetrahydrofuran (THF) as a solvent in this DFT calculation at 353.15 K temperature. The Gibbs free energies in solution phase $G(\text{sol})$ at reaction temperature were computed with the following equation (A).

$$\Delta G(\text{sol}) = \Sigma G(\text{sol}) \text{ for products} - \Sigma G(\text{sol}) \text{ for reactants} \dots \text{(A)}$$

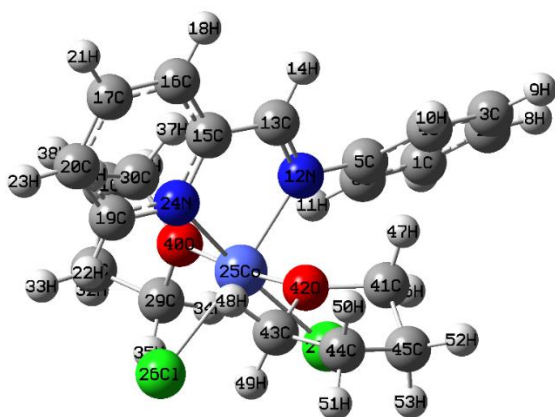


Figure S12. DFT-optimized structure of (pyrim)CoCl₂(THF)₂.

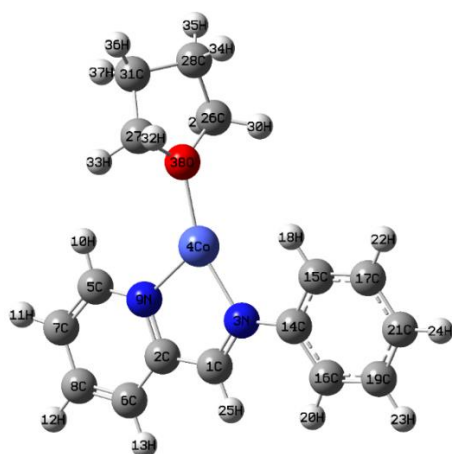


Figure S13. DFT-optimized structure of pyrim-UiO-Co(THF) (INT-1).

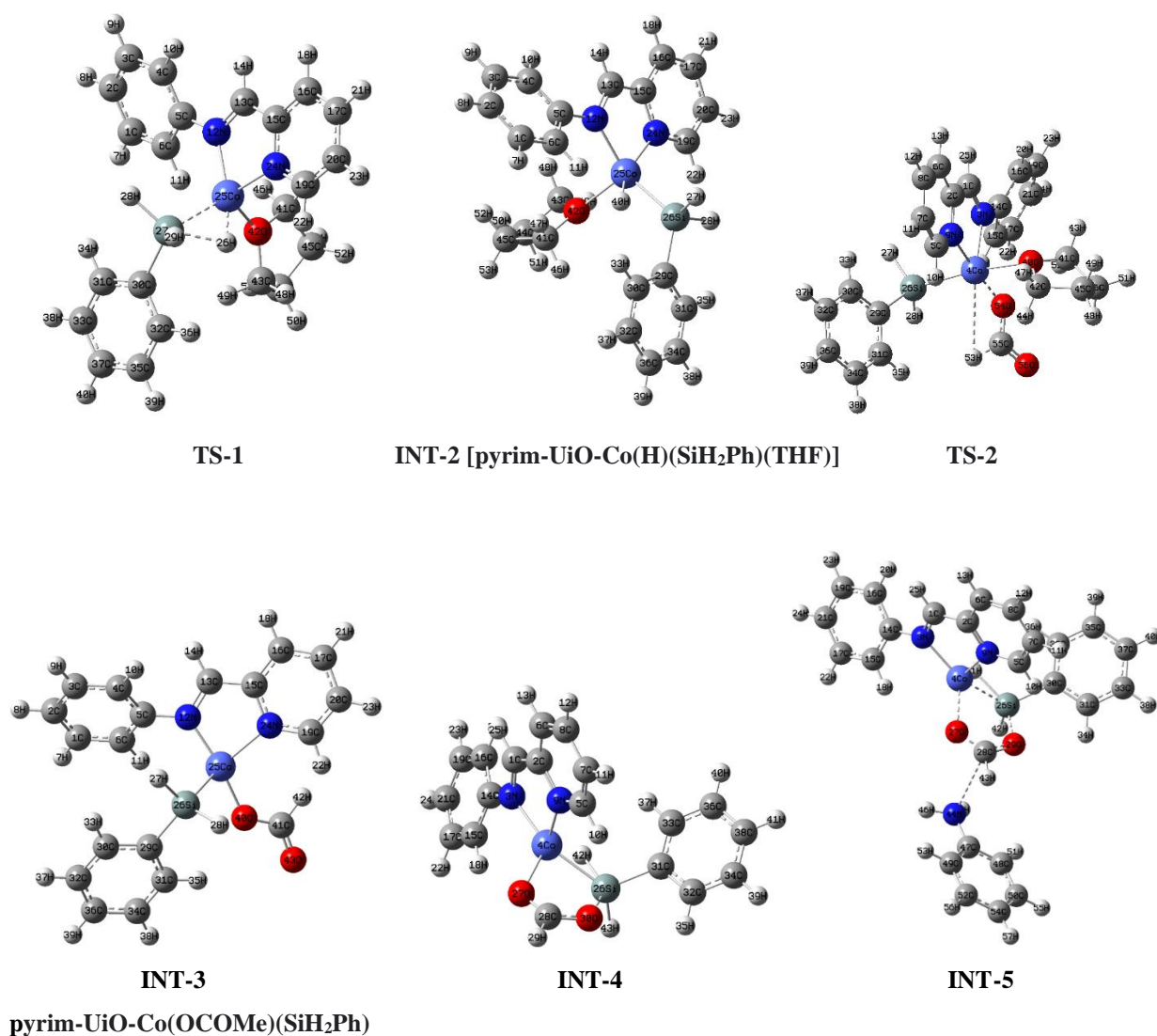


Figure S14. DFT-optimized structures of intermediates and transition states of the catalytic cycle in pyrim-UiO-Co catalysed N-formylation of benzyl amine using CO₂ and PhSiH₃.

8.1. Cartesian Coordinates of Optimized Structures

Cartesian coordinates of (pyrim)CoCl₂(THF)₂

Atom No.	Atoms	Coordinates (Angstroms)		
		X	Y	Z
1	C	-1.237099	2.771335	1.764832
2	C	0.070429	3.242726	1.885803
3	C	0.376197	4.553175	1.519128
4	C	-0.625575	5.392530	1.030095
5	C	-1.932672	4.921036	0.908734
6	C	-2.238564	3.610466	1.276492
7	H	-1.478050	1.738263	2.054397
8	H	0.859584	2.581161	2.271558
9	H	1.406656	4.924996	1.615041
10	H	-0.384237	6.425715	0.740993
11	H	-3.269117	3.239044	1.180916
12	N	-2.988274	5.804915	0.393602

13	C	-2.415042	7.121739	0.080106
14	H	-1.372874	7.303501	0.240564
15	C	-3.576187	8.017402	-0.451994
16	C	-3.140194	9.289888	-0.822344
17	C	-4.037694	10.199560	-1.381103
18	H	-2.089017	9.575855	-0.672369
19	C	-5.807343	8.564116	-1.200985
20	C	-5.371632	9.836478	-1.570833
21	H	-3.694254	11.202783	-1.672462
22	H	-6.858578	8.277661	-1.350394
23	H	-6.079083	10.553870	-2.011467
24	N	-4.909663	7.654624	-0.641159
25	Co	-4.702576	5.918370	0.047379
26	Cl	-6.839608	5.744080	-0.111420
27	Cl	-4.760357	3.884170	0.741058
28	C	-3.753559	4.252472	-3.759508
29	C	-3.422031	4.424689	-2.284218
30	H	-5.329810	5.888267	-2.809274
31	C	-4.919922	5.173359	-4.088918
32	H	-2.865433	4.502184	-4.392573
33	H	-4.023388	3.188404	-3.977088
34	H	-2.389793	4.840292	-2.163804

35	H	-3.442493	3.437401	-1.758586
36	H	-6.408551	5.698075	-2.581460
37	H	-5.208030	6.994643	-2.925437
38	H	-5.777942	4.584520	-4.500336
39	H	-4.624138	5.914817	-4.872996
40	O	-4.447735	5.373369	-1.680895
41	C	-4.268926	6.133321	3.001813
42	O	-4.877530	6.507511	1.762643
43	C	-5.911598	7.471113	1.982044
44	C	-6.005289	7.766170	3.475252
45	C	-4.941533	6.899848	4.135629
46	H	-4.398168	5.025315	3.104885
47	H	-3.178997	6.377039	2.914280
48	H	-5.638678	8.380541	1.387520
49	H	-6.858153	7.028480	1.578172
50	H	-5.821674	8.850086	3.676150
51	H	-7.023222	7.517902	3.863997
52	H	-4.197147	7.527071	4.684654
53	H	-5.398694	6.194886	4.872503

Cartesian coordinates of pyrim-Co(THF)

Atom No.	Atoms	Coordinates (Angstroms)		
		X	Y	Z
1	C	-14.055855	-5.688267	-12.732106
2	C	-13.630021	-4.603214	-11.958672
3	N	-14.374835	-5.415588	-14.024619
4	Co	-14.185806	-3.552886	-14.462666
5	C	-13.202945	-2.283393	-11.968703
6	C	-13.234667	-4.660797	-10.591816
7	C	-12.806513	-2.287849	-10.645440
8	C	-12.827835	-3.521137	-9.944848
9	N	-13.605732	-3.382893	-12.633045
10	H	-13.207626	-1.361833	-12.543424
11	H	-12.492248	-1.370001	-10.165694
12	H	-12.524565	-3.561529	-8.904373
13	H	-13.260806	-5.615861	-10.078474
14	C	-14.813048	-6.382911	-14.910811
15	C	-15.101275	-5.974445	-16.235262
16	C	-15.001559	-7.752423	-14.603391
17	C	-15.547101	-6.871471	-17.193319
18	H	-14.963245	-4.928159	-16.493752
19	C	-15.450019	-8.643654	-15.572511
20	H	-14.800637	-8.121961	-13.606010
21	C	-15.728088	-8.221409	-16.873934
22	H	-15.755868	-6.517296	-18.197517
23	H	-15.584915	-9.686975	-15.305031
24	H	-16.077034	-8.924734	-17.620844
25	H	-14.112324	-6.683830	-12.308519
26	C	-15.317565	-0.924717	-15.486769
27	C	-13.009946	-1.249122	-16.068291
28	C	-14.902184	0.156981	-16.476493
29	H	-15.464997	-0.530991	-14.477860
30	H	-16.198516	-1.491432	-15.785424
31	C	-13.378387	0.215478	-16.284784
32	H	-12.822783	-1.774594	-17.007551
33	H	-12.167193	-1.401441	-15.394939
34	H	-15.149105	-0.144313	-17.497717
35	H	-15.393550	1.108487	-16.270624
36	H	-12.857691	0.643992	-17.141736
37	H	-13.128477	0.807057	-15.400322
38	O	-14.189606	-1.850014	-15.451178

Cartesian coordinates of TS-1

Atom No.	Atoms	Coordinates (Angstroms)		
		X	Y	Z
1	C	-2.483847	1.867848	0.973635

2	C	-1.332513	1.453769	0.300282
3	C	-0.602662	2.391100	-0.431090
4	C	-1.005761	3.721567	-0.492096
5	C	-2.159712	4.152961	0.192983
6	C	-2.891428	3.194402	0.922117
7	H	-3.064114	1.154085	1.548149
8	H	-1.013739	0.418886	0.340890
9	H	0.285689	2.082187	-0.971722
10	H	-0.442548	4.421051	-1.097448
11	H	-3.770860	3.512565	1.472679
12	N	-2.625897	5.469827	0.177393
13	C	-1.816284	6.504680	-0.117787
14	H	-0.743660	6.383914	-0.223551
15	C	-2.404388	7.783748	-0.205540
16	C	-1.694195	8.994588	-0.396055
17	C	-2.374161	10.190006	-0.416631
18	H	-0.617562	8.959864	-0.515026
19	C	-4.422771	8.986158	-0.068778
20	C	-3.776226	10.195468	-0.242368
21	H	-1.838562	11.121281	-0.559872
22	H	-5.497719	8.940295	0.063459
23	H	-4.343267	11.116743	-0.248578
24	N	-3.782455	7.803967	-0.057482
25	Co	-4.494145	6.026824	0.287499
26	H	-5.864220	5.612152	0.655450
27	Si	-5.611753	5.732368	-1.086995
28	H	-4.815624	4.729167	-1.876400
29	H	-5.545679	7.010234	-1.849675
30	C	-7.374957	5.060269	-1.109080
31	C	-7.628694	3.745414	-1.530438
32	C	-8.471584	5.846658	-0.717095
33	C	-8.926087	3.233528	-1.561157
34	H	-6.802994	3.112891	-1.840784
35	C	-9.769618	5.342488	-0.749829
36	H	-8.313528	6.867997	-0.382619
37	C	-9.999298	4.032377	-1.172033
38	H	-9.098010	2.214475	-1.890267
39	H	-10.601845	5.968988	-0.447602
40	H	-11.009209	3.638164	-1.197180
41	C	-4.254096	4.858370	2.854995
42	O	-4.644979	6.040868	2.151525
43	C	-5.051114	7.059907	3.069444
44	C	-4.924406	6.524767	4.491793
45	C	-4.408277	5.099104	4.352920
46	H	-4.914172	4.030436	2.489169
47	H	-3.192362	4.646155	2.567439
48	H	-4.385612	7.942802	2.888872
49	H	-6.107851	7.326930	2.810582
50	H	-4.216892	7.151407	5.088193
51	H	-5.913813	6.544589	5.011052
52	H	-3.428678	4.974188	4.876113
53	H	-5.125598	4.367369	4.798973

Cartesian coordinates of INT-2

Atom No.	Atoms	Coordinates (Angstroms)		
		X	Y	Z
1	C	-2.281924	1.345968	0.833099
2	C	-0.886764	1.345968	0.833099
3	C	-0.189226	2.553719	0.833099
4	C	-0.886880	3.762228	0.831900
5	C	-2.281705	3.762150	0.831421
6	C	-2.979306	2.553944	0.832417
7	H	-2.831683	0.393651	0.833549
8	H	-0.337256	0.393455	0.834414
9	H	0.910454	2.553799	0.833733
10	H	-0.336680	4.714371	0.831841
11	H	-4.078910	2.554127	0.832237
12	N	-3.017028	5.035021	0.830147
13	C	-2.062061	6.152579	0.829029
14	H	-1.010027	5.957326	0.829224
15	C	-2.893787	7.472344	0.836321
16	C	-2.087348	8.610094	0.795653

17	C	-2.669568	9.875798	0.730561
18	H	-0.992573	8.508684	0.816249
19	C	-4.865021	8.866565	0.745094
20	C	-4.058846	10.004108	0.704912
21	H	-2.033998	10.772659	0.699137
22	H	-5.959967	8.967357	0.724886
23	H	-4.517677	11.002171	0.653528
24	N	-4.282480	7.600593	0.811200
25	Co	-4.615337	5.752330	0.879604
26	Si	-5.278854	5.598162	-1.370596
27	H	-4.177799	4.811187	-1.944397
28	H	-5.197744	6.982523	-1.858311
29	C	-6.974942	4.822639	-1.904871
30	C	-7.024557	3.509857	-2.374567
31	C	-8.144803	5.577396	-1.819347
32	C	-8.243703	2.952265	-2.759267
33	H	-6.101972	2.915340	-2.442598
34	C	-9.364545	5.019454	-2.203194
35	H	-8.105905	6.612029	-1.449007
36	C	-9.414157	3.707152	-2.673235
37	H	-8.282798	1.917731	-3.130088
38	H	-10.286827	5.614650	-2.135266
39	H	-10.375302	3.267277	-2.976559
40	H	-5.899533	5.062766	0.957119
41	C	-4.638930	4.674342	3.643914
42	O	-4.864961	5.692229	2.664742
43	C	-5.436203	6.854663	3.271694
44	C	-5.606593	6.600636	4.765663
45	C	-5.090297	5.188712	5.006703
46	H	-5.221213	3.774905	3.316862
47	H	-3.543606	4.440332	3.621341
48	H	-4.737307	7.705274	3.064312
49	H	-6.415332	7.039681	2.759757
50	H	-5.026975	7.347164	5.362058
51	H	-6.680332	6.691357	5.061979
52	H	-4.238508	5.190927	5.730166
53	H	-5.891864	4.535118	5.430088

Cartesian coordinates of TS-2

Atom No.	Atoms	Coordinates (Angstroms)		
		X	Y	Z
1	C	-14.662671	-11.506135	-10.067179
2	C	-14.095789	-10.648439	-9.039356
3	N	-14.997425	-10.975881	-11.191271
4	Co	-14.555447	-8.845570	-11.134577
5	C	-13.358676	-8.516018	-8.499569
6	C	-13.746832	-11.123176	-7.774615
7	C	-13.004485	-8.919150	-7.219112
8	C	-13.199815	-10.247584	-6.846292
9	N	-13.900409	-9.350965	-9.402469
10	H	-13.196121	-7.497330	-8.827946
11	H	-12.572782	-8.200345	-6.535064
12	H	-12.925228	-10.592218	-5.857299
13	H	-13.911119	-12.166023	-7.533386
14	C	-15.567114	-11.771912	-12.213331
15	C	-15.294662	-11.425894	-13.542828
16	C	-16.409665	-12.860978	-11.940447
17	C	-15.819379	-12.189309	-14.580518
18	H	-14.685016	-10.555992	-13.741245
19	C	-16.940852	-13.609310	-12.985842
20	H	-16.675132	-13.101515	-10.917755
21	C	-16.640010	-13.283805	-14.308555
22	H	-15.594704	-11.920813	-15.606331
23	H	-17.599340	-14.442071	-12.766479
24	H	-17.056440	-13.868518	-15.120559
25	H	-14.752315	-12.572218	-9.859817
26	N	-12.518789	-8.922117	-11.962927
27	H	-11.904807	-9.066155	-10.599524
28	H	-12.194922	-10.210145	-12.674005
29	C	-11.411598	-7.636547	-12.827056
30	C	-10.913516	-6.523480	-12.127255
31	C	-11.089234	-7.734400	-14.191517

32	C	-10.129537	-5.556664	-12.755403
33	H	-11.132747	-6.415065	-11.068733
34	C	-10.305494	-6.771749	-14.827996
35	H	-11.445233	-8.584795	-14.766215
36	C	-9.822505	-5.677967	-14.110726
37	H	-9.752744	-4.712140	-12.187548
38	H	-10.065999	-6.878194	-15.881082
39	H	-9.209119	-4.930056	-14.601374
40	O	-16.497539	-8.483041	-10.304447
41	C	-17.710967	-8.860987	-11.022954
42	C	-16.721465	-7.257367	-9.559530
43	H	-18.113975	-9.756918	-10.542160
44	H	-16.223073	-6.431081	-10.078157
45	C	-18.234590	-7.067821	-9.535974
46	C	-18.652878	-7.668097	-10.886149
47	H	-16.276080	-7.377423	-8.571117
48	H	-18.515433	-6.019483	-9.424608
49	H	-18.677402	-7.632327	-8.710701
50	H	-18.476451	-6.951740	-11.692849
51	H	-19.701715	-7.966879	-10.915529
52	H	-17.429130	-9.082668	-12.049665
53	H	-14.745161	-6.366697	-12.779386
54	O	-15.302345	-8.319282	-12.816338
55	C	-15.403430	-7.114410	-13.273804
56	O	-16.146171	-6.759372	-14.180467

Cartesian coordinates of INT-3

Atom No.	Atoms	Coordinates (Angstroms)		
		X	Y	Z
1	C	-2.212744	1.578881	0.000141
2	C	-0.817584	1.578881	0.000141
3	C	-0.120046	2.786632	0.000141
4	C	-0.817700	3.995141	-0.001058
5	C	-2.212525	3.995063	-0.001537
6	C	-2.910126	2.786857	-0.000541
7	H	-2.762503	0.626564	0.000591
8	H	-0.268076	0.626368	0.001456
9	H	0.979634	2.786712	0.000775
10	H	-0.267500	4.947284	-0.001117
11	H	-4.009730	2.787040	-0.000721
12	N	-2.947848	5.267933	-0.002811
13	C	-1.992881	6.385492	-0.003929
14	H	-0.940847	6.190238	-0.003734
15	C	-2.824607	7.705257	0.003363
16	C	-2.018168	8.843007	-0.037305
17	C	-2.600388	10.108710	-0.102397
18	H	-0.923393	8.741596	-0.016709
19	C	-4.795841	9.099477	-0.087864
20	C	-3.989666	10.237021	-0.128047
21	H	-1.964818	11.005571	-0.133822
22	H	-5.890787	9.200269	-0.108072
23	H	-4.448498	11.235084	-0.179430
24	N	-4.213300	7.833505	-0.021758
25	Co	-4.546157	5.985243	0.046646
26	Si	-5.852382	5.285513	-1.751424
27	H	-5.133180	4.248545	-2.505311
28	H	-6.127082	6.429935	-2.632184
29	C	-7.526591	4.561094	-1.091240
30	C	-7.709518	3.179755	-1.021159
31	C	-8.547394	5.421168	-0.686539
32	C	-8.913259	2.658696	-0.547106
33	H	-6.904828	2.501958	-1.341016
34	C	-9.751197	4.900109	-0.211391
35	H	-8.403322	6.509904	-0.741540
36	C	-9.934328	3.519113	-0.141745
37	H	-9.057750	1.569922	-0.492428

38	H	-10.555726	5.578481	0.108013
39	H	-10.883326	3.108046	0.232049
40	O	-5.437892	5.523676	1.564593
41	C	-5.075818	6.416681	2.621165
42	H	-4.385747	7.212614	2.433572
43	O	-5.565982	6.269660	3.770815

9	N	-13.944120	-6.705986	-10.573162
10	H	-13.508987	-4.751572	-10.067839
11	H	-13.042974	-5.213862	-7.686554
12	H	-13.269826	-7.585243	-6.844811
13	H	-13.930732	-9.363054	-8.447679
14	C	-14.969481	-9.481353	-13.369130
15	C	-14.697225	-9.170618	-14.715797
16	C	-15.660645	-10.679757	-13.098969
17	C	-15.079715	-10.024337	-15.742419
18	H	-14.160963	-8.256791	-14.946656
19	C	-16.040666	-11.529998	-14.133416
20	H	-15.928477	-10.933863	-12.081014
21	C	-15.752351	-11.215316	-15.460971
22	H	-14.848264	-9.760525	-16.768746
23	H	-16.576770	-12.443302	-13.897914
24	H	-16.051795	-11.881003	-16.261984
25	H	-14.520746	-10.012914	-10.810380
26	Si	-15.103459	-4.517148	-12.818040
27	O	-12.533113	-5.654006	-13.130101
28	C	-12.468686	-4.427367	-12.983046
29	O	-13.489882	-3.676980	-12.710265
30	C	-16.119300	-3.700767	-11.475245
31	C	-15.970861	-2.335715	-11.174698
32	C	-17.074338	-4.438808	-10.757784
33	C	-16.751541	-1.730884	-10.192547
34	H	-15.236655	-1.740285	-11.706935
35	C	-17.861729	-3.833560	-9.779841
36	H	-17.199959	-5.497637	-10.957801
37	C	-17.700984	-2.478663	-9.495794
38	H	-16.621394	-0.677179	-9.971870
39	H	-18.594909	-4.419942	-9.237364
40	H	-18.310409	-2.007209	-8.732862
41	H	-15.734808	-6.119531	-13.056209
42	H	-15.475810	-3.978998	-14.154207
43	H	-11.515549	-3.901353	-13.054837
44	N	-12.208727	-3.599717	-15.771203
45	H	-13.110776	-3.314620	-16.126737
46	H	-11.911739	-4.476316	-16.177337
47	C	-11.236232	-2.596023	-15.755845
48	C	-11.602883	-1.241459	-15.701088
49	C	-9.870717	-2.923401	-15.722061
50	C	-10.630440	-0.249711	-15.619224
51	H	-12.653980	-0.972271	-15.723665
52	C	-8.906554	-1.922966	-15.640671
53	H	-9.570931	-3.965783	-15.762901
54	C	-9.275032	-0.578760	-15.587989
55	H	-10.937247	0.790043	-15.581682
56	H	-7.857861	-2.199374	-15.620065
57	H	-8.521228	0.197028	-15.525870

Cartesian coordinates of INT-4

Atom No.	Atoms	Coordinates (Angstroms)		
		X	Y	Z
1	C	-14.055015	-8.642455	-11.153012
2	C	-13.630420	-7.637684	-10.242637
3	N	-14.392881	-8.299809	-12.406589
4	Co	-14.157673	-6.333373	-12.600172
5	C	-13.168238	-5.359004	-9.872945
6	C	-13.247246	-7.922999	-8.906753
7	C	-12.783171	-5.584382	-8.565582
8	C	-12.828752	-6.910981	-8.075420
9	N	-13.584725	-6.329295	-10.706476
10	H	-13.156091	-4.357735	-10.291762
11	H	-12.460745	-4.760679	-7.942113
12	H	-12.535905	-7.127062	-7.054245
13	H	-13.290887	-8.948648	-8.557105
14	C	-14.782042	-9.220937	-13.366961
15	C	-15.286025	-8.703577	-14.579874
16	C	-14.715715	-10.626310	-13.233807
17	C	-15.707438	-9.537482	-15.604582
18	H	-15.343188	-7.625357	-14.685472
19	C	-15.139460	-11.455159	-14.267555
20	H	-14.318174	-11.072166	-12.330600
21	C	-15.639115	-10.926110	-15.459230
22	H	-16.091733	-9.103939	-16.521809
23	H	-15.073775	-12.531083	-14.142019
24	H	-15.964268	-11.581154	-16.258974
25	H	-14.106968	-9.667457	-10.797293
26	Si	-16.001057	-5.073187	-13.217049
27	O	-13.153787	-5.573932	-13.953023
28	C	-13.731304	-4.562377	-14.782559
29	H	-13.127657	-4.053902	-15.505030
30	O	-15.032418	-4.272657	-14.596973
31	C	-16.522345	-3.980409	-11.701234
32	C	-15.917128	-2.740514	-11.494248
33	C	-17.502247	-4.434192	-10.818386
34	C	-16.291310	-1.954944	-10.404252
35	H	-15.144078	-2.383384	-12.190016
36	C	-17.877359	-3.648069	-9.728564
37	H	-17.979482	-5.411320	-10.981474
38	C	-17.271993	-2.408670	-9.521297
39	H	-15.813869	-0.977912	-10.240684
40	H	-18.650290	-4.005934	-9.032875
41	H	-17.566899	-1.789076	-8.661977
42	H	-16.663115	-6.373519	-13.038959
43	H	-17.133424	-4.538935	-13.987256

Cartesian coordinates of INT-5

Atom No.	Atoms	Coordinates (Angstroms)		
		X	Y	Z
1	C	-14.416988	-8.973322	-11.103827
2	C	-14.065280	-8.011660	-10.129945
3	N	-14.553055	-8.579681	-12.381919
4	Co	-14.315394	-6.604463	-12.590201
5	C	-13.584911	-5.762345	-9.682541
6	C	-13.824580	-8.333448	-8.769900
7	C	-13.327511	-6.019986	-8.350009
8	C	-13.457613	-7.347540	-7.885586

9. XPS analysis. All the binding energies were corrected with reference to the C1s peak at 284.8 eV. MULTIPAK software was used for peak analysis and de-convolution studies.

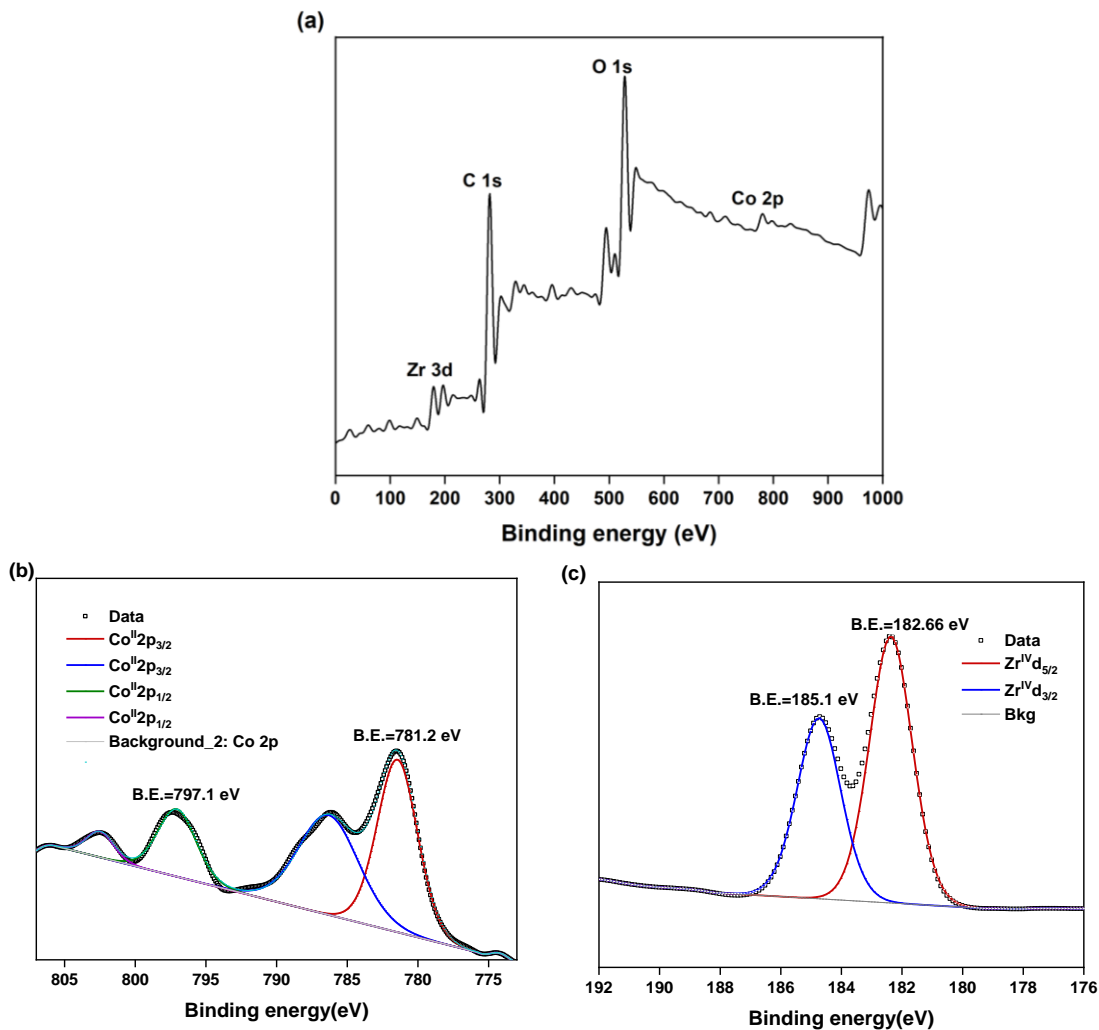


Figure S15. (a) XPS data of pyrim-UiO-CoCl₂. (b) Co 2p XPS spectrum of pyrim-UiO-CoCl₂. (c) Zr 3d XPS spectrum of pyrim-UiO-CoCl₂.

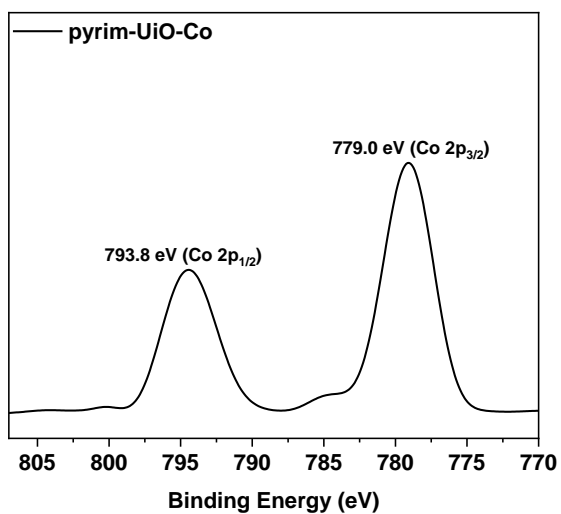


Figure S16. Co 2p XPS spectrum of pyrim-UiO-Co(THF).

Table S9. Comparison of catalytic activity of pyrim-UiO-Co(THF) with that of other reported heterogeneous catalysts in N-formylation of amines with CO₂.

Sl no.	Reference	Catalyst	Conditions	Productivity	%Yield of N-Formaldehyde
1	New J. Chem., 2021,45, 9501-9505	Zn(OAc) ₂ on mesoporous organosilica	1 mmol amine, CO ₂ (5 bar), PhSiH ₃ (1 mmol), 1 mol% Catalyst, 60° C, 17 h, CH ₃ CN		33-86%
2	ACS Sustainable Chem. Eng., 2020, 8, 14, 5576–5583	Ru-PPh ₃ -SO ₃ Na@POPs	1 mmol amine, CO ₂ (30 bar), H ₂ (30 bar), 0.4 mol% Catalyst, 100° C, 48 h, DMI	TON 250	30-80%
3	Chem. Cat. Chem., 2018, 10, 22, 5124-5127	Mg-Al layered double hydroxide supported Pd catalyst	1 mmol amine, CO ₂ (30 bar), H ₂ (30 bar), 1 mol% Catalyst, 140° C, 16 h, CH ₃ OH		88-97%
4	Sci. China Chem., 2018, 61, 725–731	Pd/N-doped carbon nanocatalysts	1 mmol amine, CO ₂ (30 bar), H ₂ (40 bar), 20 mg (2 mol%) Catalyst, 130° C, 24 h, ethanol	TON 247	11-99%
5	Chem. Asian J., 2018, 13, 20, 3018-3021	NHC-Ir coordination assembly	10 mmol amine, CO ₂ (30 bar), H ₂ (30 bar), 0.1 mol% Catalyst, 100° C, 20 h, CH ₃ OH	TON 990	53-97%
6	Inorganica Chim. Acta., 2020, 501, 119274	UiO-66 MOF	5 mmol amine, CO ₂ (10 bar), DMAB (1.5 eq.), 10 mg (0.3 mol%) Catalyst, 60° C, 12 h, DMF		30-94%
7	New J. Chem., 2017, 41, 2869-2872	CarPy-CMP@Ru (Pyridine-functionalized organic porous polymers)	1 mmol amine, CO ₂ (40 bar), H ₂ (40 bar), 0.5 mol% Catalyst, 130° C, 24 h, CH ₃ OH	TON 188	89-91%
8	Chem. Cat. Chem., 2017, 9, 11, 1939-1946	Pd NPs@Hyperscrosslinked Microporous Polymer	1 mmol amine, CO ₂ (10 bar), Diphenylmethylsilane (2.5 mmol), 50 mg (0.5 mol%) Catalyst, 60° C, 20 h, dioxane+water		79-97%
9	Catal. Lett., 2018, 148, 2487–2500	FeNi ₃ /KCC1/APTPOSS/TCT/PVA/Cu(II) MNPs (Copper(II) Complex-Based FeNi ₃ /KCC-1)	10 mmol amine, CO ₂ (15 bar), H ₂ (20 bar), 18 mg Catalyst, 90° C, 1.5 h, dioxane		58-96%

10	ACS Sustainable Chem., Eng. 2017, 5, 3, 2516–2528	Pd–Au@Polyaniline-Functionalized CNs	1 mmol amine, CO ₂ (35 bar), H ₂ (35 bar), 50 mg (Pd 1.6 wt %, Au 3.0 wt %) Catalyst, 125° C, 48 h, dioxane		0.1-95%
11	Chem. Cat. Chem., 2017, 9, 19, 3632-3636	Au NPs@TiO ₂	0.5 mmol amine, CO ₂ (20 bar), H ₂ (30 bar), 4.5 mol% Catalyst, 100-140° C, 5-20 h, DMA		91-99%
12	Chin. J. Catal., 2019, 40, 8, 1141-1146	Pd/PAL catalyst (PAL-Palygorskite)	1 mmol amine, CO ₂ (10 bar), H ₂ (30 bar), 0.35 mol% Catalyst, 96° C, CH ₃ OH	TON 283	76-99%
13	ACS Sustainable Chem., Eng., 2021, 9, 48, 16153-16162	Pd _{0.25} Cu _{0.75} /Al ₂ O _{3-0.1}	1 mmol amine, CO ₂ (20 bar), H ₂ (40 bar), 60 mg Catalyst, 150° C, 3 h, THF	TON 527	8-99%
14	Appl. Catal. B., 2021, 294, 5, 120238	Zn-TpPa (Zn single atom catalyst@COF)	CO ₂ (10 bar), phenylsilane(2 eq.), 30° C, 18 h, DMF	TON 51467	79-99%
15	ACS Sustainable Chem., Eng., 2017, 5, 7, 5758–5765	Nano-Pd/C in situ reduction of Pd(NH ₃) _x Cl _y /C	1mmol amine, 10/30 bar CO ₂ /H ₂ , 50mg Pd/C, 0.5 mmol KOH, 5 h, CH ₃ OH		27-51%
16	Chem. Eur. J., 2018, 24, 16588	Porous organic polymers with inbuilt NHCs	0.5 mmol amine, 0.75 mmol phenylsilane, CO ₂ (4 bar), 25° C, 24 h, THF		22-98%
17	Adv. Synth. Catal. 2021, 363, 1335	Ru/POP ₃ -Py&PPh ₃	1 mmol amine, 16.5 mg of catalyst, CO ₂ (20 bar), H ₂ (20 bar), 100° C, 24 h		67-99%
18	Asian J. Org. Chem. 2022, 11, e202200064	PdNPore	1 mmol amine, 2.7 mg of catalyst, 2 mmol phenylsilane, CO ₂ (10 bar), 36 h, MeCN/H ₂ O		32-86%
19	This work	Pyrim-UiO-Co(THF)₂ MOF	0.375 mmol amine, CO₂ (1 bar), phenylsilane (0.750 mmol), 80° C, 16 h, THF	TON up to 6000	41-99%

10. References

1. J. H. Cavka, S. Jakobsen, U. Olsbye, N. Guillou, C. Lamberti, S. Bordiga and K. P. Lillerud, *J. Am. Chem. Soc.*, 2008, **130**, 13850-13851.
2. T. Zhang, K. Manna and W. Lin, *J. Am. Chem. Soc.*, 2016, **138**, 3241-3249.
3. C.-C. Cao, C.-X. Chen, Z.-W. Wei, Q.-F. Qiu, N.-X. Zhu, Y.-Y. Xiong, J.-J. Jiang, D. Wang and C.-Y. Su, *J. Am. Chem. Soc.*, 2019, **141**, 2589-2593.
4. R. Newar, N. Akhtar, N. Antil, A. Kumar, S. Shukla, W. Begum and K. Manna, *Angew. Chem. Int. Ed.*, 2021, **60**, 10964-10970.
5. R. Newar, W. Begum, N. Antil, S. Shukla, A. Kumar, N. Akhtar, Balendra and K. Manna, *Inorg. Chem.*, 2020, **59**, 10473-10481.
6. J. Casado, M. A. Lopez-Quintela and F. M. Lorenzo-Barral, *J. Chem. Educ.*, 1986, **63**, 450.
7. A. K. Poswal, A. Agrawal, A. K. Yadav, C. Nayak, S. Basu, S. R. Kane, C. K. Garg, D. Bhattachryya, S. N. Jha and N. K. Sahoo, *AIP Conf. Proc.*, 2014, **1591**, 649-651.
8. B. Ravel and M. Newville, *J Synchrotron Radiat*, 2005, **12**, 537-541.
9. H. Park, E. N. Brothers and K. M. Merz, *J. Am. Chem. Soc.*, 2005, **127**, 4232-4241.
10. T. Vreven, K. S. Byun, I. Komáromi, S. Dapprich, J. A. Montgomery, Jr., K. Morokuma and M. J. Frisch, *J. Chem. Theory Comput.*, 2006, **2**, 815-826.
11. M. Araújo, B. Lasorne, A. L. Magalhães, G. A. Worth, M. J. Bearpark and M. A. Robb, *J. Chem. Phys.*, 2009, **131**, 144301.
12. V. Yempally, S. J. Kyran, R. K. Raju, W. Y. Fan, E. N. Brothers, D. J. Darensbourg and A. A. Bengali, *Inorg. Chem.*, 2014, **53**, 4081-4088.
13. S. Canneaux, F. Bohr and E. Henon, *J. Comput. Chem.*, 2014, **35**, 82-93.
14. M. Friedrichs, R. Zhou, S. R. Edinger and R. A. Friesner, *J. Phys. Chem. B*, 1999, **103**, 3057-3061.
15. B. Marten, K. Kim, C. Cortis, R. A. Friesner, R. B. Murphy, M. N. Ringnalda, D. Sitkoff and B. Honig, *J. Phys. Chem.*, 1996, **100**, 11775-11788.